Dynamic Response of a Single Interface in a Biocomposite Structure

B. Bar-On,[1] B. Bayerlein,[2] H. Blumtritt,[3] and I. Zlotnikov[2,*]
[1]Department of Mechanical Engineering, Ben-Gurion University of the Negev, Beer-Sheva 84105, Israel
[2]Department of Biomaterials, Max Planck Institute of Colloids and Interfaces, Potsdam 14476, Germany
[3]Max Planck Institute of Microstructure Physics, 06120 Halle, Germany
(Received 21 June 2015; published 2 December 2015)

Biological composite materials are known to be tough, stiff, stable, viscoelastic bodies, that can creep, recover, absorb energy, and filter vibrations. Their multifunctionality is associated with their architectures, which often consist of mineral units surrounded by organic interfaces that play a key role in the performance of the entire composite. However, the confinement and small dimensions of these organic interfaces pose a challenge in measuring their physical properties by direct methods. We propose an indirect, experimental-analytical framework by which to probe the elastic and viscoelastic behavior of an individual interface. We demonstrate this framework on thin organic interfaces in the shell *Pinna nobilis*, and discuss its possible uses in various other micro- and nanoscale composite systems.

DOI: 10.1103/PhysRevLett.115.238001 PACS numbers: 81.05.Lg, 62.23.Pq, 81.07.Pr, 81.70.Bt

Nature is successful in forming complex hierarchical composite architectures with strength and toughness that are superior to those of the constituent materials [1]. In many cases, these biocomposites exhibit a viscoelastic behavior leading to a time-dependent mechanical functionality, such as the ability to recover [2], absorb impacts [3], filter mechanical signals [4,5], or reduce vibrations [6]. The strategy that is often being employed in the formation of mineral-organic biocomposites is the use of a softer and dissipative organic phase as a continuous matrix that glues together much stiffer and more brittle mineral components, resulting in a composite material that possesses a high mechanical efficiency [7]. For instance, the microstructure of shells with prismatic, nacreous, or crossed-lamellar architectures consists of calcium carbonate building blocks (in the form of prisms, platelets, and fibers, respectively) surrounded by an organic matrix [8]. The mineral units are relatively large, whereas the thickness of the organic material varies from less than 50 nm (in the case of the nacreous and crossed-lamellar structures) to 1 μm (in the case of the prismatic assembly). While the stiffer component provides general stiffness to the composite and carries most of the load, the softer gluing organic interfaces play a key role in providing the mechanical superiority of these structures [1,7,9,10]. In fact, although the organic interfaces comprise only a very small volume fraction of these materials, their physical properties strongly affect the macroscopic stiffness, strength, toughness, and deformability of the entire biocomposite material.

The mechanical characterization of small-scale structural features in complex composite materials is experimentally challenging. Currently, the most direct experimental approach for probing the local static and time-dependent mechanical response of complex composite materials with a high lateral resolution (<50 nm) is by using nanoindentation instrumentation [11] equipped with a nanoscale dynamic mechanical analysis (nanoDMA) technique utilized in the modulus mapping mode [12–17]. Nevertheless, applying this approach to confined nanometer-scale structural features in composite materials presents a unique difficulty, mainly because the standard Hertz assumptions [18], which form the theoretical basis for the modulus mapping method, become invalid. Consequently, proper quantification of the local physical properties becomes complicated and requires the support of finite element analysis [14] and even modifications of the theory behind the technique [19]. Therefore, except for nanoindentation-based surface techniques (and similar atomic force microscopy-based techniques [20]), there is currently no viable *in situ* methodology to directly measure the static and dynamic mechanical response of an individual submicrometer-thick interface. The development of such new approaches is essential so as to gain a deeper understanding of the structural and mechanical superiority of biological and engineered composite materials.

In this Letter, we present an indirect experimental-analytical framework developed for (but not limited to) quantifying the elastic and viscoelastic properties of a single organic interface in biocomposite materials. The methodology is based on force modulation of a microcantilever that contains an individual organic interface and is cut out from the biocomposite by using the focused ion beam (FIB) milling technique. During measurement, a modulating force is applied by standard nanoindentation instrumentation, equipped with nanoDMA, at different locations along the microcantilever, far from the interface. The resulting time-dependent flexural deflection of the microcantilever is used, by applying a theoretical treatment, to extract the elastic modulus and the damping coefficient of the interface alone. We demonstrated this method on the calcite-organic composite prismatic structure in the bivalve

shell *Pinna nobilis* (*P. nobilis*) [21]. The combination of nanoindentation instrumentation with FIB has already been shown to be an effective tool for characterizing the mechanical properties of various milled structures; the most common examples are the compression tests of microscopic pillars [22,23] and the bending experiments of microcantilevers [24,25], all excavated from the investigated materials by using the FIB technique. Nevertheless, these experiments were unable to extract mechanical properties beyond the linear elasticity and plasticity of homogeneous materials.

The prismatic layer in *P. nobilis* comprises elongated calcitic prisms glued together by an approximately 1-μm thick organic matrix, Fig. 1(a). This microstructure was chosen due to the relatively thick organic interface. It allows validating the proposed methodology by comparing the results obtained by microcantilever modulation experiments to those obtained by direct measurement of the elastic modulus and the damping coefficient of the organic phase through standard nanoDMA. In a transverse cut parallel to the surface of the shell, Fig. 1(b), the prismatic layer exhibits a rather uniform honeycomb pattern with the prisms [bright areas in Fig. 1(b)] held together by the organic glue [dark interfaces in Fig. 1(b)]. In the longitudinal cut, an interlocking assembly of elongated prisms is evident, Fig. 1(c). A scanning electron microscopy (SEM) image of a microcantilever, milled from a transverse cut of the prismatic layer, is shown in Fig. 1(d) (see also Supplemental Material [26]). Its moment of inertia I, calculated based on its pentagonal shape and dimensions measured in SEM, is 1.36 μm^4. This microcantilever was used in the experiments described below.

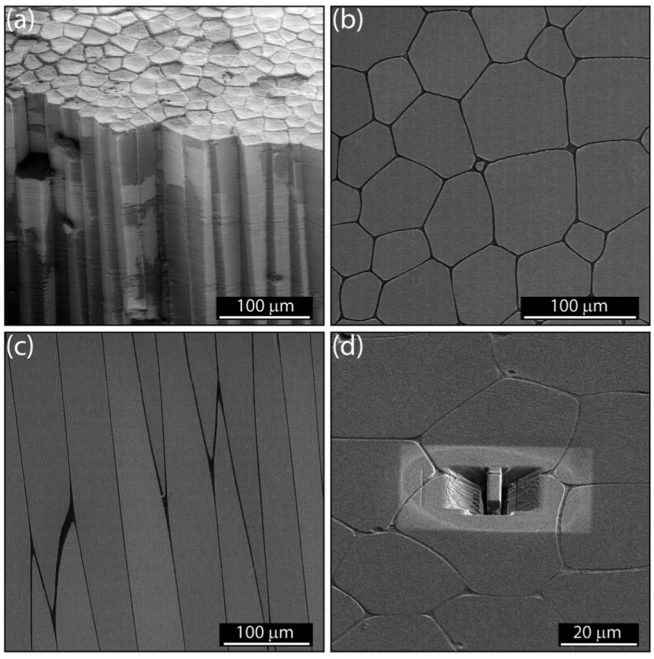

FIG. 1. Scanning electron micrographs of the prismatic layer of the shell of *P. nobilis*. (a) General view on the prismatic layer. (b) A transverse section, parallel to the surface of the shell. (c) A longitudinal section, perpendicular to the surface of the shell. (d) The microcantilever, milled from a transverse section, which was used in the forced modulation experiments (sample tilted by 52°).

For a high lateral precision, a two-dimensional topographical map (30 × 30 μm) of the surface of the sample was obtained by the nanoindenter. In Fig. 2(a), the topography of the microcantilever with a single interprismatic interface, presented in Fig. 1(d), is shown. During measurements, a small static contact force, $F_S = 10$ μN, was applied onto the microcantilever by using a diamond Berkovich tip at three different distances—$L_f = 3.5$, 6.5, or 8.5 μm—from the organic interface. Because of the small contact force, an elastic bending of the microcantilever was realized with no plastic deformation involved. Then, a periodic modulating force with an amplitude $F = 3$ μN and a frequency $f = \omega/2\pi$, varying from 1 to 300 Hz, was applied in addition to F_S. The resulting displacement amplitude of the modulating tip-microcantilever configuration, measured at three distances as a function of the angular frequency, ω, is presented in Fig. 2(c). From a systematic shift of the angular resonance frequency values (where the displacement amplitude is at maximum), the increase of the effective stiffness of the experimental configuration with decreasing L_f is already evident.

In this experiment, the displacement amplitude U_0, under the periodic force $F\exp(i\omega t)$, equals

$$|U_0| = \frac{F}{\sqrt{(K - m\omega^2)^2 + (\omega C)^2}}, \tag{1}$$

where m is the effective mass, and C and K are the effective damping and stiffness of the specific tip-microcantilever configuration, respectively (see Supplemental Material [26]). From Eq. (1) it can be seen that with the aid of the parameter $|U_0|$ measured at different frequencies, one can extract the stiffness K and the damping C for a given experimental configuration, i.e., for a specific distance from the organic interface. To decouple the contribution of the microcantilever and of the indenter tip to the calculated stiffness and damping, a Kelvin-Voigt mechanical equivalents model [schematically illustrated in Fig. 2(b)] is used [19]. In this model

$$K = K_i + K_b, \qquad C = C_i + C_b, \tag{2}$$

where K_i and C_i are the stiffness and damping of the free indenter, respectively, known from a system calibration procedure ($K_i = 376.26$ N/m, $C_i = 0.1247$ Ns/m). Parameters K_b and C_b are the stiffness and damping of the microcantilever, respectively. By using Eq. (1), the experimental data were fitted toward extracting the

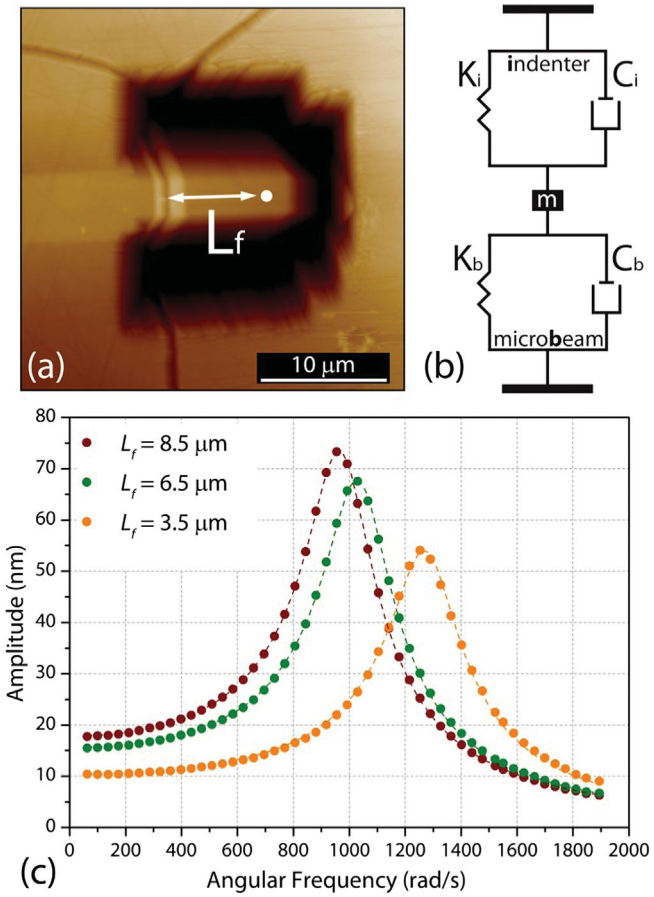

FIG. 2 (color). Forced modulation experiments. (a) Topography map of the microcantilever measured by using the nanoindenter with a contact force of 2 μN. (b) Kelvin-Voigt mechanical equivalents model of the indenter tip-microcantilever configuration. (c) Displacement amplitude of the modulating tip-microcantilever configuration as a function of angular frequency, measured at three distances.

parameters K and C [dashed lines in Fig. 2(c)]. These values were introduced into Eq. (2) to obtain the effective microcantilever parameters K_b and C_b at three different distances L_f (Table I).

To isolate the contribution of the organic interface, with thickness $L_o = 1$ μm, from the mechanical behavior of the entire microcantilever, we consider the applied force to comprise two portions, F_K and F_C ($F = F_K + F_C$), resulting in microcantilever deflection δ and velocity $\dot{\delta}$, respectively, Fig. 3(a), which are linearly related via K_b and C_b:

TABLE I. Geometrical and mechanical properties of the tip-microcantilever configuration.

L_f (μm)	K (N/m)	C (Ns/m)	K_b (N/m)	C_b (Ns/m)	η (μm^3)
3.5	964.7	0.1454	588.5	0.02072	15.75
6.5	641.1	0.1426	264.8	0.01798	48.75
8.5	561.8	0.1406	185.6	0.01576	80.75

$$F_K = K_b\delta, \qquad F_C = C_b\dot{\delta}. \tag{3}$$

In addition, two assumptions are made: (i) The viscoelastic properties of calcite are negligible as compared to the organic phase, and the calcite material is analytically rigid; (ii) the viscoelastic mechanical behavior of the organic material follows the fundamental Kelvin-Voigt solid model [27];

$$\sigma = E\varepsilon + D\dot{\varepsilon}, \tag{4}$$

where σ is the stress, ε and $\dot{\varepsilon}$ are the strain and strain rate, respectively, and E and D are the elastic modulus and damping coefficient of the organic material, respectively. The mechanical behavior of the microcantilever is governed by the organic material; thus, the force portions F_K and F_C and the moment portions $M_K = F_K L_f$ and $M_C = F_C L_f$, applied to the edge of the organic layer, which are obtained by force and moment equilibrium considerations, determine the time-dependent flexural deflection of the microcantilever. By employing the Timoshenko beam theory [28], analytical correlations are extracted between the applied forces and the moments on the organic layer, and the total microcantilever deflection and the velocity at the point of force application (see Supplemental Material [26]). The following relations are obtained for the elastic modulus and the damping coefficient of the organic material (E and D) as a function of the stiffness and damping coefficients of the microcantilever (K_b and C_b), respectively:

$$\frac{1}{K_b}IE = \left[\frac{L_o^3}{3} + \kappa\frac{E}{G}\frac{I}{A}L_o\right] + (L_o^2 L_f) + (L_o L_f^2), \tag{5}$$

and

$$\frac{1}{C_b}ID = \left[\frac{L_o^3}{3} + \kappa\frac{D}{S}\frac{I}{A}L_o\right] + (L_o^2 L_f) + (L_o L_f^2), \tag{6}$$

where G and S are the shear modulus and shear damping of the organic material, respectively, A and I are the cross sectional area and the moment of inertia of the microcantilever, respectively, and k is the shear intensity factor. It can be seen that, due to the linearity of the Kelvin-Voigt solid model, the general form of Eq. (6), which is derived from microcantilever velocity considerations, is similar to the formulation of Eq. (5), which is derived from microcantilever deflection (the viscoelastic beam theory [29]).

By employing unconventional scaling, a linear correlation between the geometric properties of the indenter tip-microcantilever configuration (L_o, L_f) and mechanical properties of the organic interface (E, D) is obtained. Exchanging variables with $x_K = 1/K_b$, $x_C = 1/C_b$, and $y = L_f L_o^2 + L_f^2 L_o = \eta$ yields the following linear relationships:

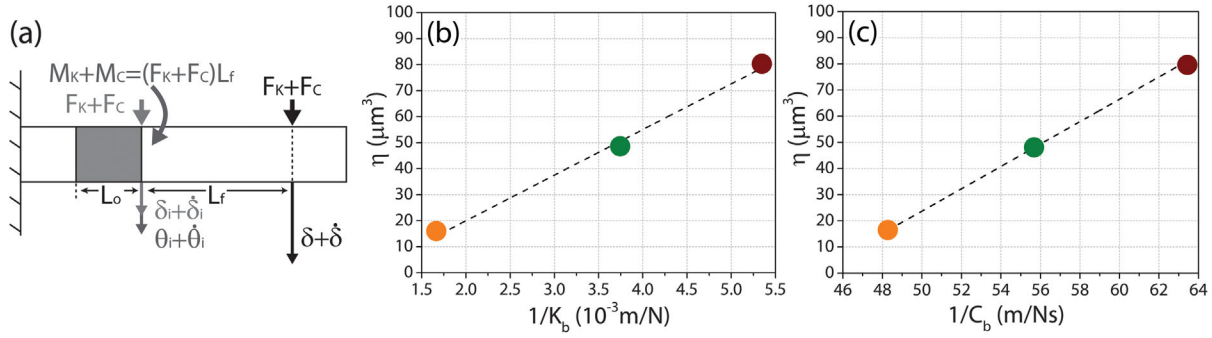

FIG. 3 (color). Elastic modulus and damping coefficient of the organic interface. (a) Schematic representation of the force-modulation experiment. (b) Calculation of the elastic modulus. Circles represent the experimental stiffness data adapted from Table I, and the dashed line represents the linear fit. (c) Calculation of the damping coefficient. Circles represent the experimental damping data adapted from Table I, and the dashed line represents the linear fit.

$$a_K x_K + b_K = y, \qquad a_K = IE, \qquad b_K = \left[\frac{L_o^3}{3} + \kappa \frac{E}{G}\frac{I}{A} L_o\right], \tag{7}$$

and,

$$a_C x_C + b_C = y, \qquad a_C = ID, \qquad b_C = \left[\frac{L_o^3}{3} + \kappa \frac{E}{S}\frac{I}{A} L_o\right]. \tag{8}$$

Note that such a scaling eliminates the need to calculate shear deformations, which are very difficult to handle. The experimental stiffness and damping data adapted from Table I are plotted according to Eq. (7) and Eq. (8) in Figs. 3(b) and 3(c), respectively. In both cases, the data provide an excellent linear fit with a regression coefficient R^2 greater than 0.99. The slopes of the fitted lines are $a_K = 1.73 \times 10^{-14}$ N m^2 and $a_C = 4.26 \times 10^{-18}$ N m^2 s. The elastic modulus and the damping coefficient are obtained from $E = a_K/I$ and $D = a_C/I$, respectively, by substituting the calculated moment of inertia I, yielding $E = 12.7$ GPa and $D = 0.0031$ GPa s.

To confirm the predictions of the developed methodology, the mechanical properties of the organic interface were also measured directly by using the nanoDMA technique. At least 10 measurements were performed with a static force of 200 μN and a dynamic force of 10 μN applied with a frequency ranging from 1 to 300 Hz. The resulting elastic modulus (assuming a Poisson's ratio in the range between 0.3 and 0.4) is between 11.6 ± 3.5 GPa and 12.8 ± 3.5 GPa, and the resulting damping coefficient is 0.0028 ± 0.0002 GPa s [11]. Those values provide an excellent fit to the mechanical properties obtained by the developed force modulation experiment and, thus, validate the experimental and analytical framework presented.

The method described in this Letter provides a novel experimental tool with the capacity for shedding light on the role of organic interfaces in the unique static and dynamic performance of bulk mineral-organic biocomposite structures. This method can be used to probe much thinner interfaces in a variety of biological composites, such as thin organic interfaces in siliceous spicules in marine sponges [30] or different organic layers in wood cell walls [31]. It can also be used to study synthetic lamellar composites, such as lamellar eutectic materials [32] or engineered structures [33], where a direct measurement of mechanical properties is not possible. Most importantly, the experimental and theoretical concepts presented in this Letter can be further developed to study other structural submicron features in complex composite materials.

B. B-O. and B. B. contributed equally to this work.

*To whom all correspondence should be addressed.
igor.zlotnikov@mpikg.mpg.de.

[1] U. G. K. Wegst, H. Bai, E. Saiz, A. P. Tomsia, and R. O. Ritchie, Nat. Mater. **14**, 23 (2015).
[2] M. J. Harrington, H. S. Gupta, P. Fratzl, and J. H. Waite, J. Struct. Biol. **167**, 47 (2009).
[3] J. Taylor and M. Layman, Palaeontology **15**, 73 (1972).
[4] S. L. Young, M. Chyasnavichyus, M. Erko, F. G. Barth, P. Fratzl, I. Zlotnikov, Y. Politi, and V. V. Tsukruk, Acta Biomater. **10**, 4832 (2014).
[5] M. Erko, O. Younes-Metzler, A. Rack, P. Zaslansky, S. L. Young, G. Milliron, M. Chyasnavichyus, F. G. Barth, P. Fratzl, V. Tsukruk, I. Zlotnikov, and Y. Politi, J. R. Soc. Interface **12** (2015).
[6] H. C. Spatz, A. Emanns, and O. Speck, J. Bionic Eng. **1**, 149 (2004).
[7] J. W. C. Dunlop, R. Weinkamer, and P. Fratzl, Mater. Today **14**, 70 (2011).
[8] S. Mann, *Biomineralization* (Oxford University Press, New York, 2001).
[9] H. Gao, B. Ji, I. L. Jäger, E. Arzt, and P. Fratzl, Proc. Natl. Acad. Sci. U.S.A. **100**, 5597 (2003).
[10] B. Bar-On and H. D. Wagner, J. Struct. Biol. **183**, 149 (2013).
[11] W. C. Oliver and G. M. Pharr, J. Mater. Res. **7**, 1564 (1992).

[12] S. A. Syed Asif, K. J. Wahl, R. J. Colton, and O. L. Warren, J. Appl. Phys. **90**, 1192 (2001).
[13] I. Zlotnikov, A. Masic, Y. Dauphin, P. Fratzl, and E. Zolotoyabko, Adv. Eng. Mater. **16**, 1073 (2014).
[14] I. Zlotnikov, D. Shilo, Y. Dauphin, H. Blumtritt, P. Werner, E. Zolotoyabko, and P. Fratzl, R. Soc. Chem. Adv. **3**, 5798 (2013).
[15] H. Ryou, E. Romberg, D. H. Pashley, F. R. Tay, and D. Arola, J. Mech. Behav. Biomed. Mater. **42**, 229 (2015).
[16] G. Balooch, G. W. Marshall, S. J. Marshall, O. L. Warren, S. A. Syed Asif, and M. Balooch, J. Biomech. **37**, 1223 (2004).
[17] H. Moshe-Drezner, D. Shilo, A. Dorogoy, and E. Zolotoyabko, Adv. Funct. Mater. **20**, 2723 (2010).
[18] K. L. Johnson, *Contact Mechanics* (Cambridge University Press, Cambridge, England, 1985).
[19] I. Zlotnikov, P. Fratzl, and E. Zolotoyabko, J. Appl. Phys. **116**, 114308 (2014).
[20] S. R. Cohen and E. Kalfon-Cohen, Beilstein J. Nanotechnol. **4**, 815 (2013).
[21] B. Bayerlein, P. Zaslansky, Y. Dauphin, A. Rack, P. Fratzl, and I. Zlotnikov, Nat. Mater. **13**, 1102 (2014).
[22] D. Jang, X. Li, H. Gao, and J. R. Greer, Nat. Nanotechnol. **7**, 594 (2012).
[23] J. Schwiedrzik, R. Raghavan, A. Bürki, V. LeNader, U. Wolfram, J. Michler, and P. Zysset, Nat. Mater. **13**, 740 (2014).
[24] M. G. Mueller, V. Pejchal, G. Žagar, A. Singh, M. Cantoni, and A. Mortensen, Acta Mater. **86**, 385 (2015).
[25] D. Kupka, N. Huber, and E. T. Lilleodden, J. Mech. Phys. Solids **64**, 455 (2014).
[26] See Supplemental Material at http://link.aps.org/supplemental/10.1103/PhysRevLett.115.238001 for a schematic representation of the experimental set-up, detailed calculation of the displacement amplitude and of the static and dynamic microcantilever deflection.
[27] R. M. Christensen, *Theory of Viscoelasticity. An Introduction* (Academic Press, New York, 1971).
[28] S. Timoshenko and J. M. Gere, *Mechanics of Materials* (Van Nostrand Reinhold Co., New York, 1972).
[29] H. F. Brinson and L. C. Brinson, *Polymer Engineering Science and Viscoelasticity: An Introduction* (Springer Science & Business Media, New York, 2007).
[30] J. Aizenberg, J. C. Weaver, M. S. Thanawala, V. C. Sundar, D. E. Morse, and P. Fratzl, Science **309**, 275 (2005).
[31] L. Bertinetti, U. D. Hangen, M. Eder, P. Leibner, P. Fratzl, and I. Zlotnikov, Philos. Mag. **95**, 1992 (2015).
[32] W. F. Smith and J. Hashemi, *Foundations of Materials Science and Engineering* (McGraw-Hill, 2006).
[33] I. Zlotnikov, A. Dorogoy, D. Shilo, I. Gotman, and E. Y. Gutmanas, Adv. Eng. Mater. **12**, 935 (2010).